Geophysical Research Letters

RESEARCH LETTER
10.1029/2022GL098752

Key Points:

- Lamb wave produced by the volcanic eruption excites the sea surface as it travels across the Pacific and generates a tsunami pulse
- The effect of the air-sea coupling becomes weaker as the Lamb wave approaches the coast
- The tsunami wave splits when passing the continental slope of Japan causing more complex waves

Supporting Information:

Supporting Information may be found in the online version of this article.

Correspondence to:

M. Yamada,
masumi@eqh.dpri.kyoto-u.ac.jp

Citation:

Yamada, M., Ho, T.-C., Mori, J., Nishikawa, Y., & Yamamoto, M.-Y. (2022). Tsunami triggered by the Lamb wave from the 2022 Tonga volcanic eruption and transition in the offshore Japan region. *Geophysical Research Letters*, *49*, e2022GL098752. https://doi.org/10.1029/2022GL098752

Received 18 MAR 2022
Accepted 27 JUL 2022

Author Contributions:

Conceptualization: Masumi Yamada, Tung-Cheng Ho, Jim Mori, Masa-Yuki Yamamoto
Data curation: Tung-Cheng Ho, Yasuhiro Nishikawa, Masa-Yuki Yamamoto
Formal analysis: Masumi Yamada, Tung-Cheng Ho
Methodology: Masumi Yamada
Resources: Tung-Cheng Ho, Yasuhiro Nishikawa, Masa-Yuki Yamamoto
Supervision: Jim Mori
Visualization: Masumi Yamada
Writing – original draft: Masumi Yamada
Writing – review & editing: Tung-Cheng Ho, Jim Mori, Yasuhiro Nishikawa, Masa-Yuki Yamamoto

Tsunami Triggered by the Lamb Wave From the 2022 Tonga Volcanic Eruption and Transition in the Offshore Japan Region

Masumi Yamada[1], Tung-Cheng Ho[1], Jim Mori[1], Yasuhiro Nishikawa[2], and Masa-Yuki Yamamoto[2]

[1]Disaster Prevention Research Institute, Kyoto University, Uji, Japan, [2]School of System Engineering, Kochi University of Technology, Kami, Japan

Abstract The 2022 volcanic eruption in Tonga caused an unusually large tsunami around the Pacific. It travels with a faster apparent velocity and has larger amplitudes at long distances than what would be expected from a conventional tsunami from the volcanic source. This tsunami was generated by the moving atmospheric Lamb wave and traveled at the speed of the Lamb wave (0.31 km/s). Japanese data showed the amplitude of this first tsunami becomes small when approaching the coast, due to the weaker air-sea coupling at the shallow depth. This wave split when passing the continental slope, and traveled at the speed of the ocean gravity wave. Therefore, the tsunami observed at the coast is delayed by thousands of seconds from the passage of the Lamb wave. Tsunamis generated by this atmospheric mechanism have not been previously observed by modern digital recording systems and should be considered in the tsunami warning systems.

Plain Language Summary A tsunami is usually generated by the sudden changes of the water heights, and caused by offshore earthquakes, coastal landslides, and submarine volcanic eruptions. The generated vertical displacement of the water propagates as a very long wave, and the tsunami waves become compressed with increased heights as they approach the coast. The 2022 volcanic eruption in Tonga caused an unusually large tsunami, which cannot be explained by conventional sources. The speed and amplitude are very different from theoretical values: the speed is about 0.31 km/s, whereas the average tsunami speed in the Pacific is 0.2 km/s. These data suggest that the tsunami from the Tonga eruption was excited by a pulse of atmospheric pressure as it traveled from the volcano. This source of the tsunami in the atmosphere needs to be considered for the tsunami warning system in the future.

1. Introduction

The large eruption at Hunga Tonga-Hunga Ha'apai volcano in Tonga at about 04:15 on 15 January 2022 (UTC) caused a surprisingly large tsunami in Japan, the west coasts of North and South America along with other regions around the Pacific (Carvajal et al., 2022; Kubota et al., 2022; Lynett, 2022; Matoza et al., 2022; United States Geological Survey, 2022). The tsunami was also observed in the oceans separated by continents from the source region such as the Atlantic and Mediterranean (Carvajal et al., 2022). For example, the Japan Meteorological Agency (JMA) initially announced that there was no danger of a significant tsunami in Japan. Several hours later when tsunami heights of 1.2 m were observed at southern islands (Kominato in Amami city), a tsunami warning was issued at 15:15 (UTC) with evacuation procedures for coastal regions over the country (Japan Meteorological Agency, 2022; TBS NEWS DIG Powered by JNN, 2022).

Rapid analysis revealed that the tsunami was generated by the atmospheric pressure wave from the volcanic eruption (Kubota et al., 2022; Kulichkov et al., 2022; Lynett, 2022; Matoza et al., 2022; Watanabe et al., 2022). Two major atmospheric waves are involved; the atmospheric Lamb wave, a non-dispersive atmospheric wave traveling along the earth's surface horizontally at the speed of 0.31 km/s (Lamb, 1881; Nishida et al., 2014; Press & Harkrider, 1962), and some modes of the acoustic gravity waves traveling at the speed 0.2–0.22 km/s (Harkrider & Press, 1967; Kubota et al., 2022; Press & Harkrider, 1966). Since the average tsunami speed in the Pacific Ocean is close to these waves (about 0.2 km/s), the mechanism of air-sea coupling becomes complex (Kubo et al., 2022; Kubota et al., 2022).

To understand the mechanism of this unusual tsunami, we analyzed barometer, ocean bottom pressure (OBP) gauges, and seismometer data. We first present an overview of the global feature of the atmospheric pressure wave and tsunami, then focus on the area around Japan where dense observations are available. We propose an air-sea coupling mechanism for tsunami generation which is associated with a traveling air pressure wave.

2. Data and Method

2.1. Data and Preprocess

We used the atmospheric pressure, OBP, and seismic data recorded by the global and Japanese networks. The global atmospheric pressure data is provided by the Incorporated Research Institutions for Seismology (IRIS) data center. Weathernews Inc. provided the atmospheric pressure data in Japan observed by the Soratena network. The Japan Coast Guard also provided barometric pressure data measured at the ports. The global OBP waveforms were recorded at the stations of the Deep-ocean Assessment and Reporting of Tsunamis (DART) system. The Japanese OBP gauges in the Seafloor Observation Network for Earthquakes and Tsunamis along the Japan Trench (S-net) and Dense Oceanfloor Network system for Earthquakes and Tsunamis (DONET) were also used. We used tide gauge data from the Japan Coast Guard and seismic data recorded by the F-net (Full Range Seismograph Network of Japan). The list of the data set used in this study is shown in Table S1 in Supporting Information S1.

All waveform data are first converted to physical values with offsets removed. Noncausal fourth order Butterworth filters with varying corner frequencies were applied to the datasets. The atmospheric pressure data provided by the IRIS data center were high-pass filtered with a corner frequency of 0.0001 Hz to remove the long-period component associated with the earth tide. The OBP data in the DART stations were band-pass filtered with corner frequencies of 0.0001 and 0.005 Hz. For the S-net and DONET OBP data, a band-pass filter with corner frequencies of 0.0005 and 0.01 Hz was applied to detect the arrival times. A band-pass filter with corner frequencies of 0.0001 and 0.005 Hz was used for the Automated Event Location Using a Mesh of Arrays (AELUMAs) method.

2.2. AELUMA Method

We estimated the tsunami speed off the Tohoku region in Japan using an array analysis technique based on the AELUMA method (de Groot-Hedlin & Hedlin, 2015; Fan et al., 2019). We first divide the 125 S-net stations into 225 Delaunay triangle arrays (triads), and remove triads with internal angles beyond the range of 5°–175°. We used the OBP data with the band-pass filtered at 0.0001–0.005 Hz. This frequency range was selected since we focus on the velocity of the large long-period pulse in the OBP data. The AELUMA method estimates the velocity and direction of the plane wave passing the triangle by the cross-correlation of station pairs at the triangle vertices.

2.3. Tsunami Simulation With an Atmospheric Input

We performed numerical analyses of the tsunami waves using a simplified air pressure pulse with a constant water depth. The tsunami modeling was based on the linear shallow water equations, which consist of continuity equation (Equation 1) and equations of motion in two directions (Equations 2 and 3), where the atmospheric pressure was considered (e.g., Saito et al., 2021).

$$\frac{\partial \eta}{\partial t} + \frac{\partial (hu)}{\partial x} + \frac{\partial (hv)}{\partial y} = 0 \tag{1}$$

$$\frac{\partial u}{\partial t} = -\frac{\partial P_{atm}}{\rho \partial x} - g\frac{\partial \eta}{\partial x} \tag{2}$$

$$\frac{\partial v}{\partial t} = -\frac{\partial P_{atm}}{\rho \partial y} - g\frac{\partial \eta}{\partial y} \tag{3}$$

where η is water wave height, u and v are velocity along the x and y directions, h is water depth, ρ is water density, and P_{atm} is the atmospheric pressure. We defined P_{atm} as a pulse-like waveform with the amplitude of 1 hPa and the width of about 500 km moving at a constant velocity (Figure 1). The input wave height and velocity are uniform

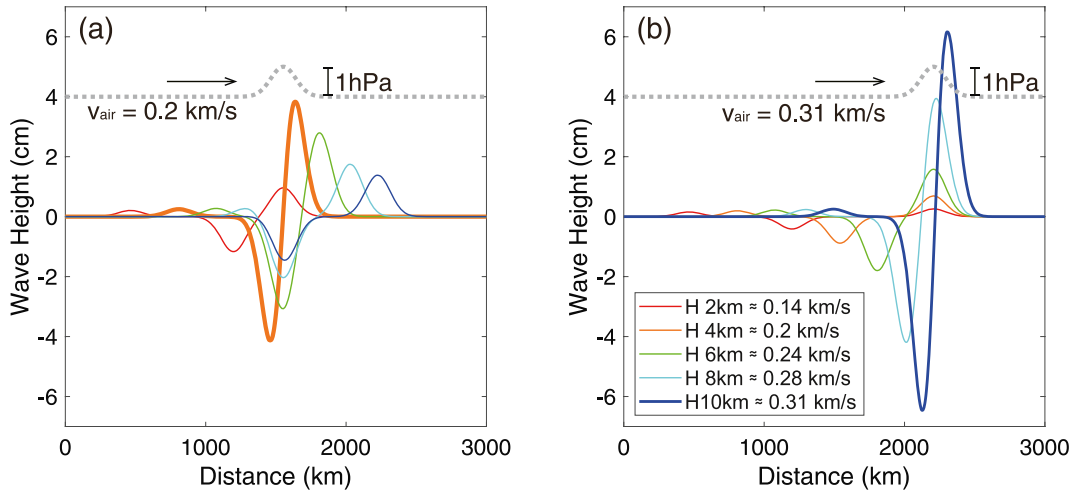

Figure 1. A snapshot of the tsunami simulations for the atmospheric pressure wave with different water depths. The velocity the atmospheric pressure wave is (a) 0.2 and (b) 0.31 km/s. The dotted line shows the waveform of the pressure wave, and colored lines show the tsunami waveforms. The thick line shows the waveform with the largest amplitude.

along the *y* direction and the profile along the *x* direction was shown in the results. We performed the simulation with various water depths (2, 4, 6, 8, and 10 km) and different pressure-wave velocities (0.2 and 0.31 km/s).

3. Results

3.1. Global Observations

Figure 2 shows the waveforms of the atmospheric and OBPs at the stations along a nearly direct path between Tonga and Japan. A single pulse-like signal in the atmospheric waveforms with a duration of about 1,500 s for the half cycle. The velocity is close to the speed of the Lamb wave (0.31 km/s). The amplitude of the positive pulse is 2–9 hPa and decays as a function of distance, but the shape is well preserved. The negative pulse propagated at a slower velocity and dispersed as it traveled. The OBP waveforms recorded at the DART stations show an initial large positive pulse (about 4 hPa and 1,500 s duration) and higher frequency oscillations for the following several hours. The shape of the first pulse is almost the same as the atmospheric pressure pulse with similar arrival times and propagation speeds.

The DART data record both the atmospheric pressure and the gravitational force due to the sea-level change. The similar initial pulses on both the barometers and DART data are most likely the strong atmospheric pressure change generated by the Tonga volcanic explosion (Figure 2b). The DART signals continue for several hours after the initial pulse, which is not seen on the barometric data, and these later signals are considered to be the tsunami traveling through the ocean.

Figure 3a shows the arrival times of the initial pulse as recorded by the barometers and the offshore DART stations around the world. The arrival times were manually picked by visual inspection (see Figure 2 and Figure S2 in Supporting Information S1 for examples of the picks). As in Figure 2, the arrival times are similar on the barometers and OBP gauges. The initial pulse traveled concentrically from Tonga. Although the depth of the seafloor varies across the Pacific, the apparent speed of the signals on the OBP gauges does not seem to be affected by the bathymetry. Figure 3c shows the arrival times of the atmospheric and OBP changes as a function of distance from the volcano. The arrival times of the atmospheric and OBP signals scale with the distance. The theoretical tsunami arrival times from the volcano based on the shallow water equation are also shown in the figure, and these calculated values are much later (about 12,000 s around Japan) than the observed arrival times.

3.2. Local Observations Around Japan

Figure 3b shows the detailed arrival times of the S-net and Soratena data around Japan. The arrival times of the initial pulse in the OBP data are almost the same as that in the barograms but slightly delayed at the stations

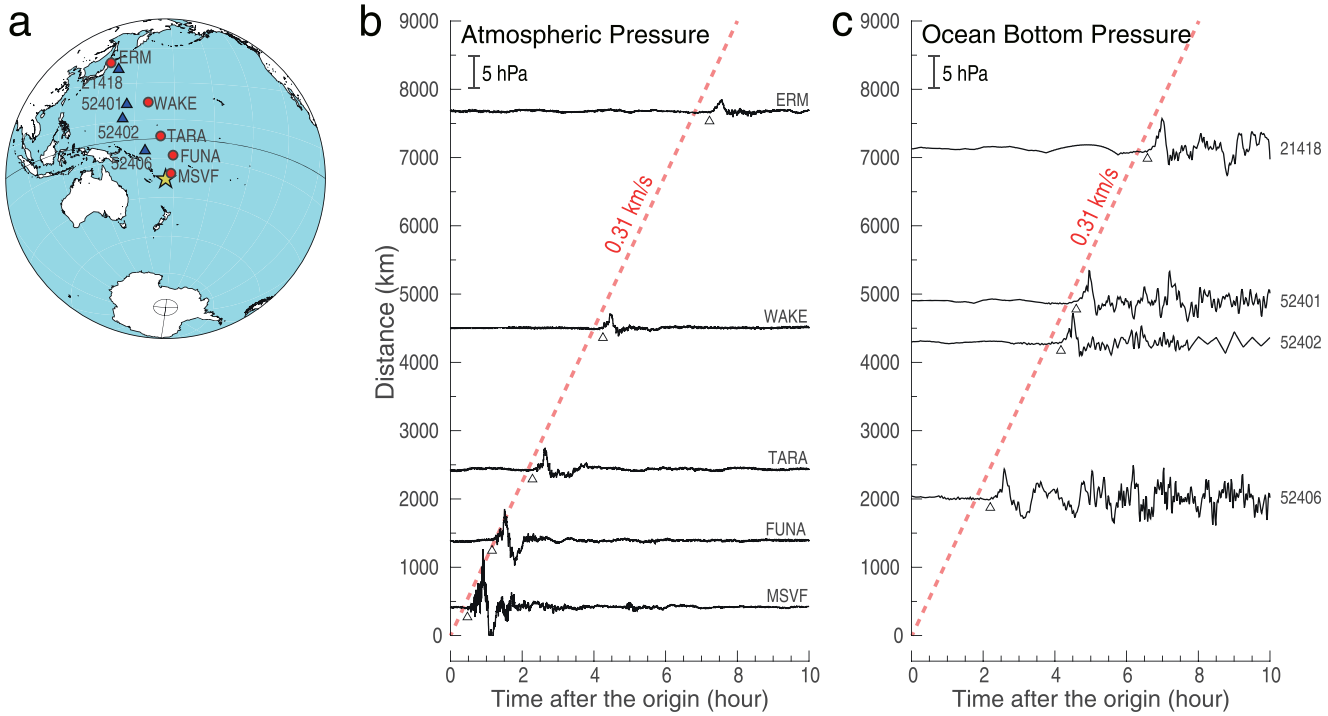

Figure 2. Atmospheric and ocean bottom pressure (OBP) waveforms in the Pacific. (a) Map of the stations. Circles show the barometric stations and triangles show the OBP stations. (b) Waveforms of the atmospheric pressure. Triangles show the manually picked arrival times. (c) Waveforms of the OBP. Triangles show the manually picked arrival times. The origin time is 4:14:45 (UTC) (United States Geological Survey, 2022).

near the coast (e.g., the color difference in the shaded area). Figure 3d shows the arrival times on the different sensors as a function of distance. The arrival times of the atmospheric and OBP changes are about the same, but the tsunami arrivals (as recorded at tide gauges that do not see the atmospheric pressure wave) are delayed by thousands of seconds (Figure S1 in Supporting Information S1).

We estimated the tsunami speed for the offshore Tohoku region in Japan using an array analysis technique based on the AELUMA method. Figure 4a shows the estimated velocity and direction of the tsunami at the center of the triad. Figure 4b shows the OBP waveform of the first tsunami pulse at the stations on the line in the east-west direction shown as a white area in Figure 4a. The waves traveling at the velocity of the Lamb wave (0.31 km/s) show a large amplitude in the deeper area, but it gradually decreases as it approaches the coast. The apparent velocity of the peak of the waveforms becomes slower at the shallower region. Figure 4c shows the relationship between the ocean depth and tsunami velocity estimated by the AELUMA method. In the area close to the trench, the tsunami velocity is similar to the Lamb wave velocity, and the tsunami velocity becomes closer to the theoretical values estimated from the shallow water approximation (i.e., $\sqrt{gh}$, where g is the gravity acceleration (9.81 m/s^2) and h is the water depth). Hereafter, we call the water wave traveling at this theoretical velocity as an ocean gravity wave.

3.3. Tsunami Simulation

Figure 1 shows the tsunami simulation for the atmospheric pressure waves traveling at the velocity of 0.2 and 0.31 km/s. The atmospheric pressure generates a water wave traveling at the speed of the air pressure pulse and a compensated wave traveling at the speed of the ocean gravity wave ($\sqrt{gh}$). The amplitude of the wave is the maximum if the velocities of the air pressure wave and the ocean gravity wave are approximately equal. The amplitude becomes smaller as the velocity of the atmospheric pressure (v_{air}) wave becomes different from the velocity of the ocean gravity wave (v_{water}).

The sign of the generated wave is also different depending on the velocities of the air pressure (input) and ocean gravity wave (medium). If the velocity of the source (v_{air}) is slower than the velocity of the medium (v_{water})

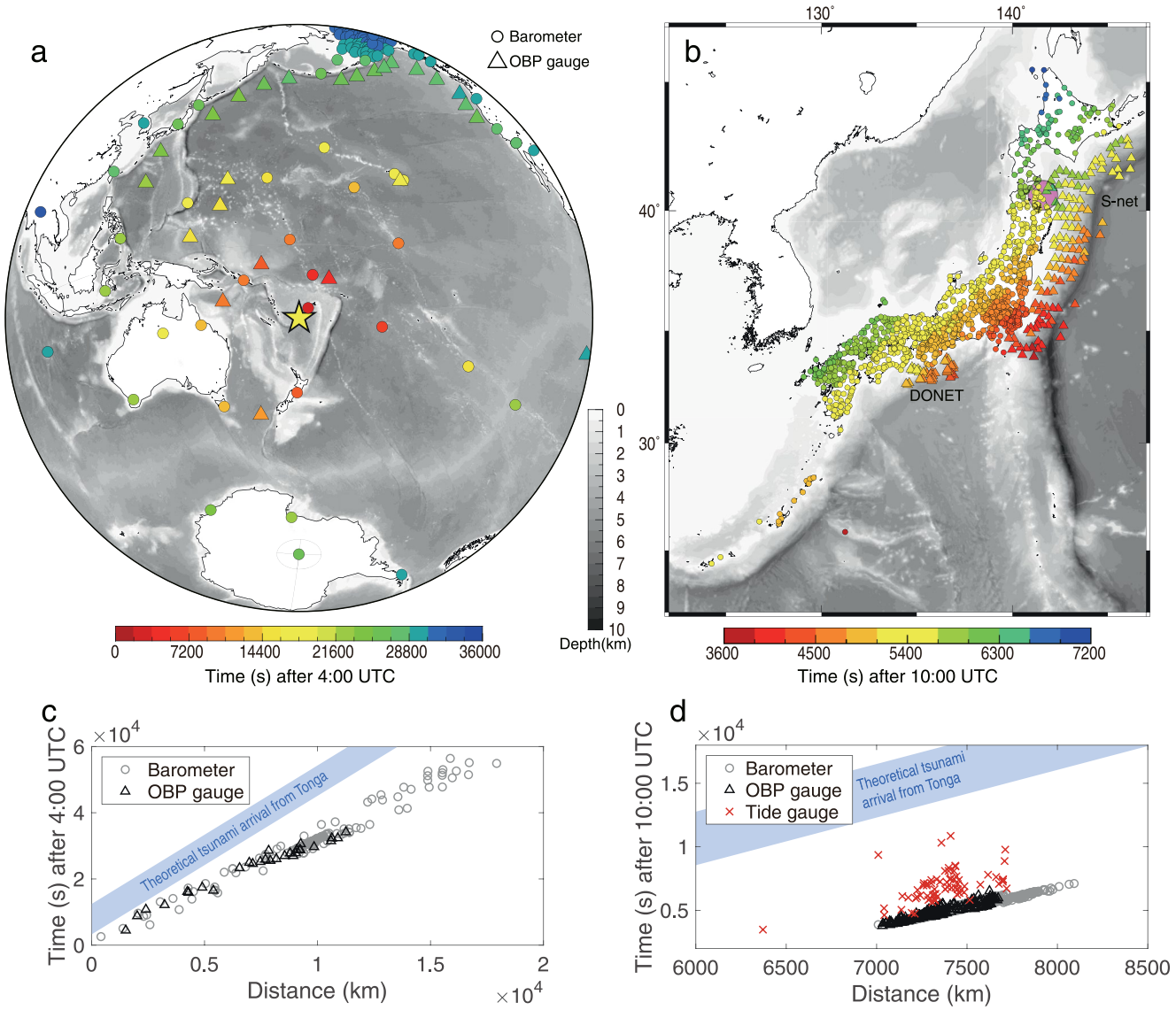

Figure 3. Arrival times of the signals on the barometers (circles) and ocean bottom pressure (OBP) gauges (triangles). (a) Global stations. A star shows the location of the volcano. (b) Regional stations around Japan. A pink shaded area (about 40N, 141E) shows the area with a large difference of the arrival times between barometers and OBP gauges. (c and d) Comparison of the arrival times on the barometers, OBP gauges, and tide gauges, as a function of distance from the volcano. Theoretical tsunami arrival times are shown as a thick blue line. (c) Global data. (d) Regional data around Japan.

(Figure 1a), the positive atmospheric pressure wave generates the negative water wave traveling at the velocity of the atmospheric pressure wave, and the preceding positive wave propagates at the velocity of the medium. If the source is faster than the velocity of the medium (Figure 1b), the positive wave travels at the velocity of the atmospheric pressure wave and the negative water wave travels at the velocity of the medium. Figure S2 in Supporting Information S1 shows the snapshot of the tsunami simulations with three different cases: (a) $v_{air} > v_{water}$ (in red line), (b) $v_{air} \approx v_{water}$ (in gray line), and (c) $v_{air} < v_{water}$ (in blue line). At the beginning of the simulation (300 s), the positive atmospheric pressure wave generates the subsidence of the sea surface for all cases, and the compensated uplifts propagate in both sides. As time passes, Case 2 amplifies the water height due to the resonance. The uplift or subsidence travels at the velocity of the atmospheric pressure wave for the cases 1 and 3, respectively.

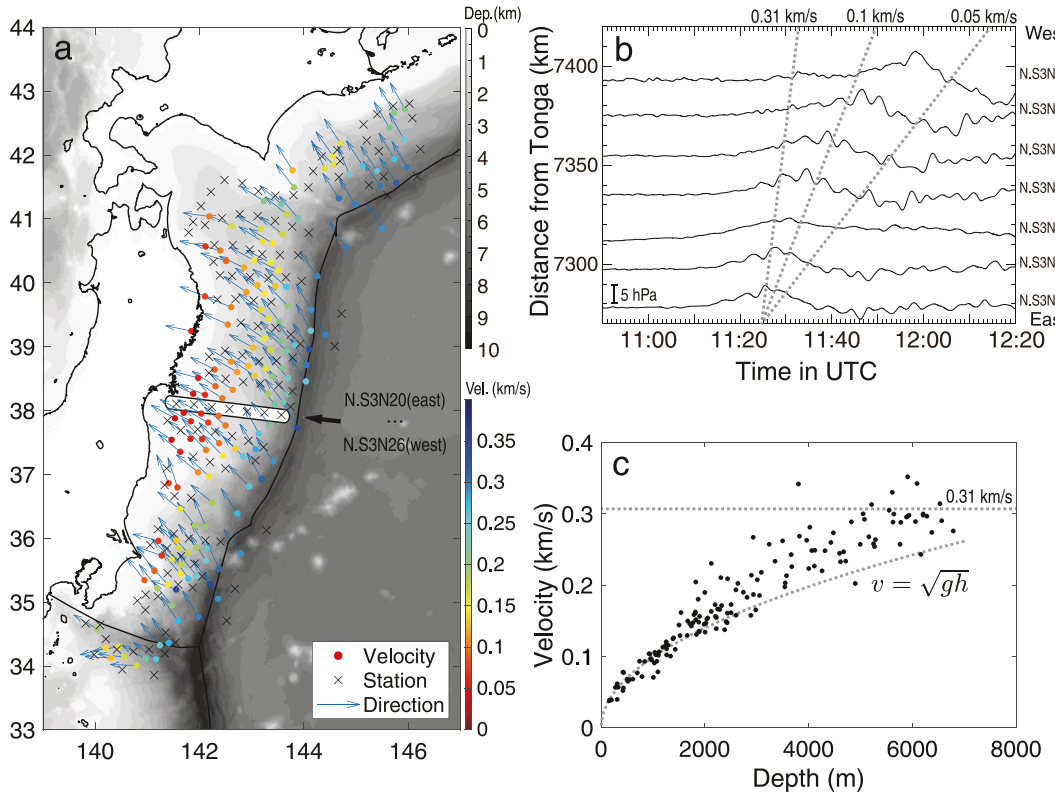

Figure 4. Tsunami velocity near the Japan coast estimated by the Automated Event Location Using a Mesh of Array method. (a) Map of the S-net stations. Cross symbols show the location of the stations. The color of the circles shows the velocity and arrows show the direction of the plane wave. The solid lines show the coastline and trench. (b) Selected S-net OBP waveforms filtered at 0.0001–0.005 Hz. The location is shown as a white area in (a) . (c) The relationship between the ocean depth and tsunami velocity at the center of the triads. The theoretical ocean gravity wave velocity and Lamb wave velocity are shown in the broken lines.

4. Discussion

4.1. Lamb Wave Generated by the Eruption

The large pulse in the barograms is a Lamb wave generated by the powerful volcanic explosion (Amores et al., 2022; Matoza et al., 2022; Otsuka, 2022). A Lamb wave is a fundamental mode of the acoustic gravity wave (Bretherton, 1969). It travels horizontally at the sound velocity and the particle motion is also only in the horizontal direction (Nishida et al., 2014). It has weak attenuation and travels a longer distance than other modes (Lindzen & Blake, 1972; Nishida et al., 2014). The pulse duration observed in Japan is about 1,500 s and its wavelength is about 465 km. The broadband seismic stations across Japan recorded very large long-period waveforms (100–500 s) at the arrival of the Lamb wave in the horizontal components (Figure S3 in Supporting Information S1) and the direction of the particle motions coincides with the direction to Tonga (Figure S4 in Supporting Information S1). These features are consistent with the characteristics of the Lamb wave. The amplitude of the Lamb wave is about 9 hPa at the closest station MSVF, where the distance from the volcano is 420 km (Figure 2a). It decays to 2 hPa in Japan, at a distance of 8,000 km. A single positive pulse was observed uniformly by over 1,300 barometers in Japan. Since the intrinsic attenuation of Lamb waves is small, the decay rate is much smaller than the simple geometrical effect of cylindrical wave propagation.

4.2. Tsunami Caused by the Air-Sea Coupling

Usually tsunamis associated with volcanic eruptions are caused by a source at the volcano such as mass movements, underwater explosions, and pyroclastic flows, and propagate through the ocean as a long wave (Grilli et al., 2019; Latter, 1981; Paris, 2015). However, the 2022 tsunami travels with a faster apparent velocity and has

larger amplitudes at long distances than what would be expected from a tsunami generated close to the volcano (see Figure S5 in Supporting Information S1 for the comparison to the 2011 Tohoku earthquake) (Lynett, 2022). Our data indicate that the first tsunami at far distances from the Tonga eruption was not generated in the region close to the volcano (as shown in Figure 3c), but was caused by a mechanism associated with the very strong explosive air phase as it traveled from the volcano (see a schematic diagram in Figure S6 in Supporting Information S1). The mechanism is similar to a meteotsunami, a water level change caused by a moving sea-surface pressure change (Hibiya & Kajiura, 1982; Kubota et al., 2021; Rabinovich, 2020; Saito et al., 2021; Šepić et al., 2015).

Kubota et al. (2022) discussed multiple factors involved in the sea surface oscillations for the following several hours after the passage of the Lamb wave. Since the first tsunami pulse generated by the Lamb wave has an apparent velocity faster than the speed of the media, the compensated water level change, traveling at the velocity of the ocean gravity wave, delays the first pulse. A classical tsunami source, such as sea-floor crustal deformations and mass movements, can also generate tsunamis traveling at the same speed (Lynett, 2022). A slower atmospheric wave, such as an acoustic gravity wave, also contributes to the amplification of tsunamis, as its velocity is closer to the average speed of a tsunami (Carvajal et al., 2022; Kubota et al., 2022; Watanabe et al., 2022; Wright et al., 2022). Watanabe et al. (2022) explained the negative pulse in Figure 2b as one of the acoustic gravity wave modes. The air-sea coupling between the acoustic gravity wave and ocean gravity wave is similar to the mechanism of Proudman resonance (matching of the speeds of ocean gravity water wave and atmospheric wave) (Hibiya & Kajiura, 1982; Šepić et al., 2015). We suggest that the large amplitude of the peak tsunami observed on the west coast of the United States and Chile is due to this resonance in the east Pacific where the depth is about 3,000–4,000 m (Carvajal et al., 2022). The observations in Japan are more complicated because of the varying water depths. DONET stations observed larger amplitudes than S-net stations at times corresponding to a velocity of 0.2 km/s (Kubo et al., 2022) since the water depth in the south-east of DONET is about 4,000 m (see Figure 4b).

A large tsunami and coseismic deformation can produce a Lamb wave in the atmosphere (Arai et al., 2011; Bowman & Shrestha, 1965; Liu et al., 2006; Mikumo, 1968; Mikumo & Watada, 2010; Watada et al., 2006). A sudden uplift of the sea surface by a tsunami produces instantaneous changes in the atmospheric pressure in the source region. The resultant pressure change propagates as a Lamb wave along the bottom boundary of the atmosphere (Watada & Kanamori, 2010). The tsunami from Tonga is a similar but opposite interaction between the atmosphere and sea surface: a large Lamb wave produced by the volcanic eruption perturbs the sea surface and leads the tsunami pulse as it travels across the ocean. This mechanism is similar to the explanation for sea-level changes associated with atmospheric pressure signals during the cataclysmic 1,883 Krakatau eruption (Ewing & Press, 1955; Harkrider & Press, 1967; Matoza et al., 2022). The Tonga case is by far the best example of such tsunamis recorded by global observation networks (Matoza et al., 2022; Poli & Shapiro, 2022). The dense barometric and OBP data was able to reveal the coupling mechanism that induced the tsunami and the contribution of the atmospheric structure and seafloor topography.

4.3. Tsunami Delay for Shallowing Water Depth

The tsunami was generated by the moving air pressure pulse as it propagated across the ocean. However, when approaching the coast, the amplitude of the tsunami with apparent velocity of the Lamb wave speed becomes smaller (a few hPa at the S-net station N.S3N26). This is because the effect of the air-sea coupling becomes weaker when the speed of the medium has a larger difference compared to the velocity of the Lamb wave (Figure 1b) (Sekizawa & Kohyama, 2022; Tanioka et al., 2022). Considering the OBP data records the change of both water height and atmospheric pressure (about 2 hPa around Japan), the tsunami traveling with apparent velocity of the Lamb wave is too small to be recorded by the tide gauge at the coast.

The tsunami velocity estimated by the AELUMA method becomes slower as it approaches the coast in Figure 4. In the area close to the trench, the estimated tsunami velocity is similar to the Lamb wave velocity. However, at the depth between 2000 and 6,000 m in Figure 4c, the water wave splits from the tsunami traveling at the speed of the Lamb wave when passing the continental slope. The split tsunami travels at the speed of the ocean gravity wave at S-net stations shallower than 2000 m (Sekizawa & Kohyama, 2022; Tanioka et al., 2022). Therefore, the tsunami measured by the tide gauges at the coast (Figure 3d and Figure S1 in Supporting Information S1) shows the delay of the arrival times is on the order of thousands of seconds after the arrival of the Lamb wave. The cross-correlation of waveforms used here determines apparent velocities which are an average for the entire

envelope. This means that the apparent velocity in deeper water is closer to the Lamb wave velocity and the apparent velocity for the shallower regions are closer to the velocity given by the shallow water equation.

5. Conclusions

The large eruption at Hunga Tonga-Hunga Ha'apai volcano in Tonga on 15 January 2022 caused a significantly large tsunami around the Pacific. We analyzed global barometric and OBP data, and Japanese local barometric, ocean pressure, and seismic data to understand the tsunami generation mechanism. We performed an array analysis based on the AELUMA method to the Japanese OBP data to estimate the tsunami speed in the offshore Tohoku region. We also performed a numerical simulation of the tsunami waves using a simplified air pressure pulse with various water depths.

The global data show that the tsunami was generated by a strong explosive air phase as it traveled from the volcano at about 0.3 km/s. Japanese OBP data showed the amplitude of the tsunami traveling with apparent velocity close to the Lamb wave speed becomes small as it approaches the coast, due to the weaker air-sea coupling at the shallow depth. It also showed the tsunami traveling at the speed of the Lamb wave split when passing the continental slope and traveling at the speed of the ocean gravity wave. This is why the tsunami measured by tide gauges on the coast are delayed by thousands of seconds.

Tsunamis generated by this atmospheric mechanism have not been observed before and have not been considered in the tsunami warning systems (Intergovernmental Oceanographic Commission, 2022). Major eruptions of once-in-a-century magnitude may cause a strong atmospheric pressure wave that triggers this type of tsunami. This mechanism is not limited to island eruptions, since an onshore eruption also causes a tsunami if the air wave is strong enough and travels across the ocean. The tsunamis generated by the massive explosion need to be considered for the tsunami warning system in the future.

Data Availability Statement

We used S-net https://doi.org/10.17598/NIED.0007, F-net https://doi.org/10.17598/NIED.0005, and Dense Oceanfloor Network system for Earthquakes and Tsunamis https://doi.org/10.17598/NIED.0008 data from the National Research Institute for Earth Science and Disaster Resilience (NIED), tsunami measurement records and AMeDAS data from the Japan Meteorological Agency (JMA) https://www.data.jma.go.jp/obd/stats/etrn/index.php, atmospheric pressure data from Weathernews Inc.'s Soratena meteorological observation sensor https://global.weathernews.com/wp-content/uploads/2022/01/20220128_1.pdf, barometric pressure data and tide gauge data from Japan Coast Guard https://near-goos1.jodc.go.jp/index.html, atmospheric pressure data from IRIS https://ds.iris.edu/ds/nodes/dmc/, and ocean bottom pressure data (DART) from National Oceanic and Atmospheric Administration https://doi.org/10.7289/V5F18WNS. The last access of all URLs is July 2022.

Acknowledgments
We would like to thank the National Research Institute for Earth Science and Disaster Resilience, Japan Meteorological Agency, Weathernews Inc., Japan Coast Guard, IRIS, and National Oceanic and Atmospheric Administration for providing their data. This study was supported by JSPS KAKENHI Grant No. 21K21353.

References

Amores, A., Monserrat, S., Marcos, M., Argüeso, D., Villalonga, J., Jordä, G., & Gomis, D. (2022). Numerical simulation of atmospheric Lamb waves generated by the 2022 Hunga-Tonga volcanic eruption. *Geophysical Research Letters*, *49*(6). https://doi.org/10.1029/2022GL098240

Arai, N., Iwakuni, M., Watada, S., Imanishi, Y., Murayama, T., & Nogami, M. (2011). Atmospheric boundary waves excited by the tsunami generation related to the 2011 great Tohoku-Oki earthquake. *Geophysical Research Letters*, *38*(7). https://doi.org/10.1029/2011GL049146

Bowman, G., & Shrestha, K. (1965). Atmospheric pressure waves from the Japanese earthquake on 16 June 1964. *Quarterly Journal of the Royal Meteorological Society*, *91*(388), 223–224. https://doi.org/10.1002/qj.49709138813

Bretherton, F. (1969). Lamb waves in a nearly isothermal atmosphere. *Quarterly Journal of the Royal Meteorological Society*, *95*(406), 754–757. https://doi.org/10.1002/qj.49709540608

Carvajal, M., Sepúlveda, I., Gubler, A., & Garreaud, R. (2022). Worldwide signature of the 2022 Tonga volcanic tsunami. *Geophysical Research Letters*, *49*(6). https://doi.org/10.1029/2022GL098153

de Groot-Hedlin, C. D., & Hedlin, M. A. (2015). A method for detecting and locating geophysical events using groups of arrays. *Geophysical Journal International*, *203*(2), 960–971. https://doi.org/10.1093/gji/ggv345

Ewing, M., & Press, F. (1955). Tide-gage disturbances from the great eruption of Krakatoa. *Eos, Transactions American Geophysical Union*, *36*(1), 53–60. https://doi.org/10.1029/TR036i001p00053

Fan, W., McGuire, J. J., de Groot-Hedlin, C. D., Hedlin, M. A., Coats, S., & Fiedler, J. W. (2019). Stormquakes. *Geophysical Research Letters*, *46*(22), 12909–12918. https://doi.org/10.1029/2019GL084217

Grilli, S. T., Tappin, D. R., Carey, S., Watt, S. F., Ward, S. N., Grilli, A. R., et al. (2019). Modelling of the tsunami from the December 22, 2018 lateral collapse of Anak Krakatau volcano in the Sunda Straits, Indonesia. *Scientific Reports*, *9*(1), 1–13. https://doi.org/10.1038/s41598-019-48327-6

Harkrider, D., & Press, F. (1967). The Krakatoa air-sea waves: An example of pulse propagation in coupled systems. *Geophysical Journal International*, *13*(1–3), 149–159. https://doi.org/10.1111/j.1365-246X.1967.tb02150.x

Hibiya, T., & Kajiura, K. (1982). Origin of the Abiki phenomenon (a kind of seiche) in Nagasaki Bay. *Journal of the Oceanographical Society of Japan*, *38*(3), 172–182. https://doi.org/10.1007/BF02110288

Intergovernmental Oceanographic Commission. (2022). Interim volcano-generated tsunami alert products and procedures of the pacific tsunami warning and mitigation system. Retrieved from https://unesdoc.unesco.org/ark:/48223/pf0000381031

Japan Meteorological Agency. (2022). Tide level changes due to a major eruption of Hunga-Tonga-Huapai volcano near the Tonga Islands at 13:00 on January 15, 2022. Retrieved from https://www.jma.go.jp/jma/press/2201/16a/kaisetsu202201160200.pdf

Kubo, H., Kubota, T., Suzuki, W., Aoi, S., Sandanbata, O., Chikasada, N., & Ueda, H. (2022). Ocean-wave phenomenon around Japan Island due to the 2022 Tonga eruption observed by the wide and dense ocean-bottom pressure gauge networks. PREPRINT (Version 1) available at Research Square. https://doi.org/10.21203/rs.3.rs-1464766/v1

Kubota, T., Saito, T., Chikasada, N. Y., & Sandanbata, O. (2021). Meteotsunami observed by the deep-ocean seafloor pressure gauge network off northeastern Japan. *Geophysical Research Letters*, *48*(21). https://doi.org/10.1029/2021GL094255

Kubota, T., Saito, T., & Nishida, K. (2022). Global fast-traveling tsunamis driven by atmospheric lamb waves on the 2022 Tonga eruption. *Science*, *377*(6601), 91–94. https://doi.org/10.1126/science.abo4364

Kulichkov, S., Chunchuzov, I., Popov, O., Gorchakov, G., Mishenin, A., Perepelkin, V., et al. (2022). Acoustic-gravity Lamb waves from the eruption of the Hunga-Tonga-Hunga-Hapai volcano, its energy release and impact on aerosol concentrations and tsunami. *Pure and Applied Geophysics*, *179*(5), 1533–1548. https://doi.org/10.1007/s00024-022-03046-4

Lamb, H. (1881). On the vibrations of an elastic sphere. *Proceedings of the London Mathematical Society*, *1*(1), 189–212. https://doi.org/10.1112/plms/s1-13.1.189

Latter, J. (1981). Tsunamis of volcanic origin: Summary of causes, with particular reference to Krakatoa, 1883. *Bulletin Volcanologique*, *44*(3), 467–490. https://doi.org/10.1007/BF02600578

Lindzen, R. S., & Blake, D. (1972). Lamb waves in the presence of realistic distributions of temperature and dissipation. *Journal of Geophysical Research*, *77*(12), 2166–2176. https://doi.org/10.1029/JC077i012p02166

Liu, J., Tsai, Y., Chen, S., Lee, C., Chen, Y., Yen, H., et al. (2006). Giant ionospheric disturbances excited by the M9.3 Sumatra earthquake of 26 December 2004. *Geophysical Research Letters*, *33*(2), L02103. https://doi.org/10.1029/2005GL023963

Lynett, P. (2022). The tsunamis generated by the Hunga Tonga-Hunga Ha'apai volcano on January 15, 2022. https://doi.org/10.21203/rs.3.rs-1377508/v1

Matoza, R. S., Fee, D., Assink, J. D., Iezzi, A. M., Green, D. N., Kim, K., et al. (2022). Atmospheric waves and global seismoacoustic observations of the January 2022 Hunga eruption, Tonga. *Science*, *377*(6601), 95–100. https://doi.org/10.1126/science.abo7063

Mikumo, T. (1968). Atmospheric pressure waves and tectonic deformation associated with the Alaskan earthquake of March 28, 1964. *Journal of Geophysical Research*, *73*(6), 2009–2025. https://doi.org/10.1029/JB073i006p02009

Mikumo, T., & Watada, S. (2010). Acoustic-gravity waves from earthquake sources. *Infrasound monitoring for atmospheric studies*, 263–279. https://doi.org/10.1007/978-1-4020-9508-5_9

Nishida, K., Kobayashi, N., & Fukao, Y. (2014). Background Lamb waves in the Earth's atmosphere. *Geophysical Journal International*, *196*(1), 312–316. https://doi.org/10.1093/gji/ggt413

Otsuka, S. (2022). Visualizing lamb waves from a volcanic eruption using meteorological satellite Himawari-8. *Geophysical Research Letters*, *49*(8). https://doi.org/10.1029/2022GL098324

Paris, R. (2015). Source mechanisms of volcanic tsunamis. *Philosophical Transactions of the Royal Society A: Mathematical, Physical & Engineering Sciences*, *373*(2053), 20140380. https://doi.org/10.1098/rsta.2014.0380

Poli, P., & Shapiro, N. M. (2022). Rapid characterization of large volcanic eruptions: Measuring the impulse of the Hunga Tonga Ha'apai explosion from teleseismic waves. *Geophysical Research Letters*, *49*(8). https://doi.org/10.1029/2022GL098123

Press, F., & Harkrider, D. (1962). Propagation of acoustic-gravity waves in the atmosphere. *Journal of Geophysical Research*, *67*(10), 3889–3908. https://doi.org/10.1029/JZ067i010p03889

Press, F., & Harkrider, D. (1966). Air-sea waves from the explosion of Krakatoa. *Science*, *154*(3754), 1325–1327. https://doi.org/10.1126/science.154.3754.1325

Rabinovich, A. B. (2020). Twenty-seven years of progress in the science of meteorological tsunamis following the 1992 Daytona Beach event. *Pure and Applied Geophysics*, *177*(3), 1193–1230. https://doi.org/10.1007/s00024-019-02349-3

Saito, T., Kubota, T., Chikasada, N. Y., Tanaka, Y., & Sandanbata, O. (2021). Meteorological tsunami generation due to sea-surface pressure change: Three-dimensional theory and synthetics of ocean-bottom pressure change. *Journal of Geophysical Research: Oceans*, *126*(5). https://doi.org/10.1029/2020JC017011

Sekizawa, S., & Kohyama, T. (2022). Meteotsunami observed in Japan following the Hunga Tonga eruption in 2022 investigated using a one-dimensional shallow-water model. *Scientific Online Letters on the Atmosphere*, *18*(0). https://doi.org/10.2151/sola.2022-021

Šepić, J., Vilibić, I., Rabinovich, A., & Monserrat, S. (2015). Widespread tsunami-like waves of 23-27 June in the Mediterranean and Black Seas generated by high-altitude atmospheric forcing. *Scientific Reports*, *5*(1), 1–8. https://doi.org/10.1038/srep11682

Tanioka, Y., Yamanaka, Y., & Nakagaki, T. (2022). Characteristics of the deep sea tsunami excited offshore Japan due to the air wave from the 2022 Tonga eruption. *Earth Planets and Space*, *74*(1), 1–7. https://doi.org/10.1186/s40623-022-01614-5

TBS NEWS DIG Powered by JNN. (2022). [JMA press conference] Tsunami warning for Iwate Prefecture, Amami Islands, and Tokara Islands. Retrieved from https://www.youtube.com/watch?v=QPIVsaZN1kA

United States Geological Survey. (2022). M 5.8 volcanic eruption - 68 km NNW of Nuku'alofa. Tonga. https://earthquake.usgs.gov/earthquakes/eventpage/us7000gc8r/executive

Watada, S., & Kanamori, H. (2010). Acoustic resonant oscillations between the atmosphere and the solid Earth during the 1991 Mt. Pinatubo eruption. *Journal of Geophysical Research*, *115*(B12), B12319. https://doi.org/10.1029/2010JB007747

Watada, S., Kunugi, T., Hirata, K., Sugioka, H., Nishida, K., Sekiguchi, S., et al. (2006). Atmospheric pressure change associated with the 2003 Tokachi-Oki earthquake. *Geophysical Research Letters*, *33*(24), L24306. https://doi.org/10.1029/2006GL027967

Watanabe, S., Hamilton, K., Sakazaki, T., & Nakano, M. (2022). First detection of the Pekeris internal global atmospheric resonance: Evidence from the 2022 Tonga eruption and from global reanalysis data. *Earth and Space Science Open Archive*. https://doi.org/10.1002/essoar.10510971.1

Wright, C. J., Hindley, N. P., Alexander, M. J., Barlow, M., Hoffmann, L., Mitchell, C. N., et al. (2022). Surface-to-space atmospheric waves from Hunga Tonga-Hunga Ha'apai eruption. *Nature*. https://doi.org/10.1038/s41586-022-05012-5